Naval Research Laboratory

Washington, DC 20375-5320

NRL/FR/5760--05--10,090

Coherent Seeker Guided Antiship Missile Performance Analysis

JAMES J. GENOVA

Integrated EW Simulation Branch
Tactical Electronic Warfare Division

January 28, 2005

REPORT DOCUMENTATION PAGE

Form Approved
OMB No. 0704-0188

1. REPORT DATE *(DD-MM-YYYY)*	**2. REPORT TYPE**	**3. DATES COVERED** *(From - To)*
28-01-2005	NRL Formal Report	January 1, 2004 through April 30, 2004

4. TITLE AND SUBTITLE

Coherent Seeker Guided Antiship Missile Performance Analysis

5a. CONTRACT NUMBER

5b. GRANT NUMBER

5c. PROGRAM ELEMENT NUMBER

6. AUTHOR(S)

James J. Genova

5d. PROJECT NUMBER

5e. TASK NUMBER

5f. WORK UNIT NUMBER

7. PERFORMING ORGANIZATION NAME(S) AND ADDRESS(ES)

Naval Research Laboratory
Washington, DC 20375-5320

8. PERFORMING ORGANIZATION REPORT NUMBER

NRL/FR/5760--05-10,090

9. SPONSORING / MONITORING AGENCY NAME(S) AND ADDRESS(ES)

Office of Naval Research (Code 313)
800 North Quincy Street
Arlington, VA 22217-5660

10. SPONSOR / MONITOR'S ACRONYM(S)

11. SPONSOR / MONITOR'S REPORT NUMBER(S)

12. DISTRIBUTION / AVAILABILITY STATEMENT

Approved for public release; distribution is unlimited.

13. SUPPLEMENTARY NOTES

14. ABSTRACT

The performance capability of an antiship missile's radar guidance system can be rated by the ratio of the processed signal level to the interference or noise level. In this report, the general performance capability is evaluated for missiles guided via noncoherent radar and for missiles guided via coherent radar. The contribution of several coherent aspects are compared including interpulse, intrapulse, and beam sharpening. Potential improvement of as much as 15 to 20 dB are indicated. A brief derivation of a useful representation of the processed signals is presented that describes the potential usefulness of Space-Time Adaptive Processing.

15. SUBJECT TERMS

Coherent pulse Doppler radar; Antiship missile; Ship defense; Electronic warfare; Space-Time Adaptive Processing

16. SECURITY CLASSIFICATION OF:			**17. LIMITATION OF ABSTRACT**	**18. NUMBER OF PAGES**	**19a. NAME OF RESPONSIBLE PERSON**
					James J. Genova
a. REPORT	**b. ABSTRACT**	**c. THIS PAGE**	UL	28	**19b. TELEPHONE NUMBER** *(include area code)*
Unclassified	Unclassified	Unclassified			(202) 767-4203

Standard Form 298 (Rev. 8-98)
Prescribed by ANSI Std. Z39.18

CONTENTS

EXECUTIVE SUMMARY

Performance capability is evaluated for antiship missiles guided via noncoherent radar and for missiles guided via coherent radar. The objectives of this report are to provide an understanding of the impact of coherent processing on the electronic battle and to provide guidance for more detailed studies. The contribution of several aspects of coherent processing are compared including interpulse, intrapulse, and beam sharpening. These aspects are investigated individually to enable a better understanding of the impact of each on performance.

The performance of an antiship missile radar guidance system is bounded by specifying the false alarm rate and the probability of detection. These specifications of system performance are expressed as the required ratio of the processed signal level to the interference level. Examples of interference sources include system noise, sea clutter, and jamming.

In the first comparison, details of each system are assumed to be equivalent. The only difference between the systems is interpulse coherent processing. That is, P pulses are coherently integrated. This is known as Doppler processing; it results in a performance improvement corresponding to the number of pulses integrated. This improvement is only manifested in noise-limited regions. The performance is not improved in clutter-limited regions. Thus, coherent processing improves missile performance for targets at particular ranges and radial speeds.

The next aspect of coherent processing reviewed is intrapulse modulation or range compression. In this case, the performance in the clutter-limited region improves by the ratio of the range resolutions. This aspect of processing has the added benefit of possibly reduced peak power levels and intrapulse modulations that render the missile more difficult to detect.

We also show that particular missile flight profiles can further improve the performance in the clutter-limited region. These flight profiles may also degrade fire control solutions for antimissile weapon systems. Possible improvements to EP (Electronic Protection) techniques made viable by use of coherent processing are mentioned.

All of these results are reviewed for a case of more realistic system parameters. Finally, a formalism is introduced that indicates how monopulse receiver channels and coherent processing might be utilized to develop a coherent prewhitening algorithm that enables further performance improvements in the clutter-limited region and against jamming.

Other features of the performance are also improved as a result of the antiship missile (ASM) use of coherent radar. Features that are expected to be improved include target discrimination, EP, and tracking. In addition, the ASM emissions have a lower probability of intercept, making the ASM more difficult to detect by the ES (Electronic Support) on the ship.

COHERENT SEEKER GUIDED ANTISHIP MISSILE PERFORMANCE ANALYSIS

BACKGROUND

This report documents an investigation of several aspects of coherent processing as it relates to the radar seeker of an antiship missile (ASM). Coherent properties of interest relate to both interpulse (Doppler) and intrapulse (range compression) capabilities. The three basic functions of the seeker required for proper ASM guidance are target detection, target discrimination, and target parameters measurement. ASM guidance performance improves with improved target detection and parameters measurement. Target detection and parameters measurement improve with higher signal-to-interference (noise, clutter, and/or jamming) ratio. Target discrimination capability also improves with higher signal-to-interference ratio and with the addition of more discrimination features. This report concentrates on the comparison of the signal-to-interference ratio of the coherent seeker processing with respect to that of a noncoherent seeker.

A difficulty with this type of comparison is that there are so many variables that it is difficult to define a valid comparison. It is assumed throughout that the ASM seeker is required to meet systems requirements as expressed by a false alarm rate and a probability of detection. To isolate the specifically coherent features, two seeker comparisons are presented. First, the two systems are assumed to have (as much as possible) identical RF component capabilities except for the effects of coherent processing. An analysis of performance is presented contrasting the relative signal-to-interference ratio required to meet system specifications. In the second comparison, the seekers are assumed to have different component capabilities, and may be representative of more realistic implementations with presently available technology. The investigations address the potentially relevant differences in performance when the *ASM is guided via a noncoherent radar seeker* vs when the *ASM is guided via a coherent radar seeker* for the same detection requirements.

These initial comparisons highlight the need to investigate the performance against targets with low relative Doppler in the presence of sea clutter. ASM processing assuming the use of sum and delta receiver channels and methods to mitigate clutter is examined in more detail. These same techniques can be useful for EP (Electronic Protection) processing, and techniques for implementing coherent processing EP are suggested.

This report shows advantages and disadvantages of the coherent seeker for identifying areas of potential interest and concern for future, more detailed analyses. It also demonstrates useful analytic approaches.

Overview

To facilitate the discussion, a simplistic scenario is hypothesized. The scenario of interest relates to a sea-skimming, radar-guided ASM flying at about Mach 1 or faster. Table 1 summarizes the scenario time line; Fig. 1 is a graphical representation (not drawn to scale). The ASM is assumed to “pop up” at long range (in excess of 50 km) from the ship for initial target detection during the Early Search mode. If necessary, the ASM goes into another Search mode for target reacquisition at a range of about 20 km from the ship.

Manuscript approved June 21, 2004.

Table 1 — Scenario Time Line

Time (s)	Time to Go (s)	Range (km)	Mode	Notes
0	300	90	Search	Pop-Up
100	200	60	Off	Coast
230	70	21	Search	Reacquire
240	60	18	Track	Guidance
300	0	0		Impact

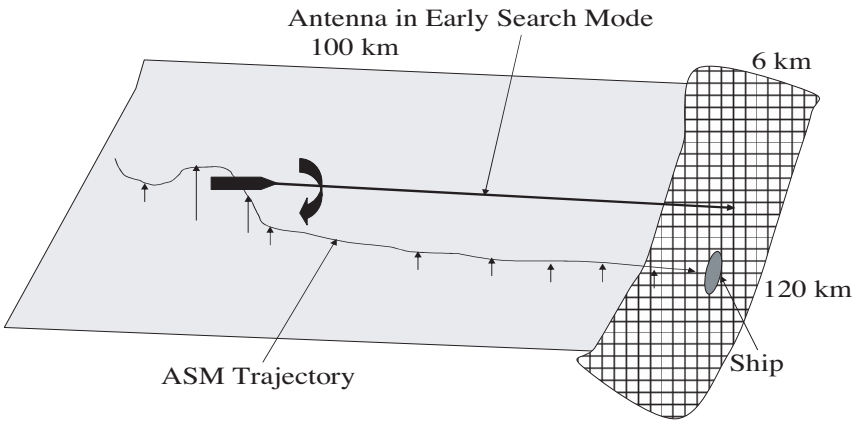

Fig. 1 — Scenario trajectory

The ship may have moved up to 3 km from its position at the start of the scenario. It is noted that an 8-deg beamwidth antenna is about 2.5 km wide at 20 km. At 80 km, a 90-deg pattern is about 120 km wide. A 6-km search swath is assumed.

After reacquiring the ship, the ASM goes into Track mode and continues guiding until impact. At each stage, the primary interest is the ASM target detection capability. Other critical aspects of the ASM performance include parameters estimation, target discrimination, and EP features including LPI (low probability of intercept). For convenience, some aspects of this scenario are admittedly overly simplistic.

The analysis procedure is to compare the scenario involving an ASM and a ship; the ASM is guided with a noncoherent radar seeker and the ASM is guided with a coherent seeker. As much as possible, it is assumed that the two systems (noncoherent-guided ASM and coherent-guided ASM) are identical except for the addition of the coherent radar capability. Figure 2 shows pertinent subsystems of both missiles. For this report, the seeker is assumed to consist of the transmitter, antenna, receiver, and RF processor. The resultant seeker data are expressed as amplitude (and possibly phase) vs position and other parameters. The seeker data are presented to the postprocessor for target detection and target parameter estimation. The parameter extraction function includes target discrimination and various EP techniques. The target parameters are then used for ASM guidance.

For this investigation, the differences between the two ASM systems relate to the details of the transmitter, receiver, and the processor, especially to the particular processing and the resultant information and information quality provided to the postprocessor by the seeker. Both systems are assumed to meet the same systems requirements as expressed by the false alarm rate and the probability of detection. As much as practical, the general capabilities of the two systems are assumed to be equivalent. After the analysis is completed for the matched systems, a comparison of more realistic systems is presented.

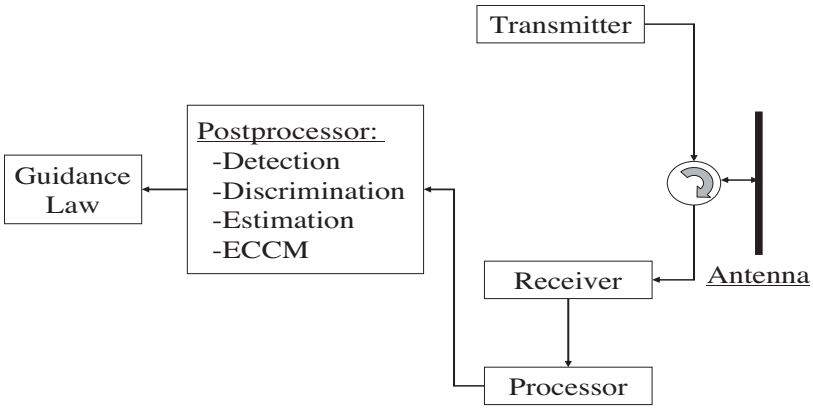

Fig. 2 — ASM functional subsystems

MATCHED SYSTEMS—ANALYSIS AND DISCUSSION

Search Mode Analysis—False Alarm Rate

The number of variables involved makes it difficult to compare the two systems. One must be careful to compare systems with maximum commonality and to only make comparisons that directly bear on the presence or nonpresence of coherent capabilities. As indicated above, the primary ASM performance relates to the ability to detect the target. To analyze the Early Search mode performance, the false alarm rate (FAR) performance requirement is first set. The average time between false alarms is 1/FAR. The probability of false alarm in a single dwell (or look) is the inverse of the number of "opportunities" (N) for a false alarm in the average time between false alarms, assuming that each opportunity is equally likely.

Figure 3 (not drawn to scale) illustrates the ocean surface search area. Assume that the radar seeker mechanically sweeps the antenna of beamwidth (θ) at a fixed sweep rate to cover an ocean surface area (A_0) in time (T_{total}) by searching multiple range swaths (labeled 1 through K in the figure). Each range swath consists of multiple subareas (A) that are geographically overlapping, and each are investigated in a single dwell time. It is further assumed that the seeker divides each dwell subarea into a number of range cells or range gates (N_{RG}).

For simplicity, it is assumed that the noncoherent seeker detection is based on data from a single pulse or that the dwell on each subarea consists of a single illumination. (The analysis could be repeated for various M of N criteria or various levels of postdetection integration.) The probability of false alarm at an individual detection cell for the noncoherent seeker (indicated throughout by the subscript I) is the inverse of the number of opportunities (N) for a false alarm in the average time between false alarms where

$$N_I = N_{RG} \cdot FAR^{-1}/dwell = N_{RG} \cdot FAR^{-1}/PRI. \tag{1}$$

Performing the same analysis for the coherent seeker (indicated throughout by the subscript C), assuming the same system performance criteria and the same range resolution, the difference is that now the system dwells on area A for multiple pulses (P) and implements Doppler processing (N_D Doppler cells) over a coherent processing interval (CPI). The number of false alarm opportunities is

$$N_C = N_{RG} \cdot N_D \cdot FAR^{-1}/dwell = N_{RG} \cdot N_D \cdot FAR^{-1}/CPI. \tag{2}$$

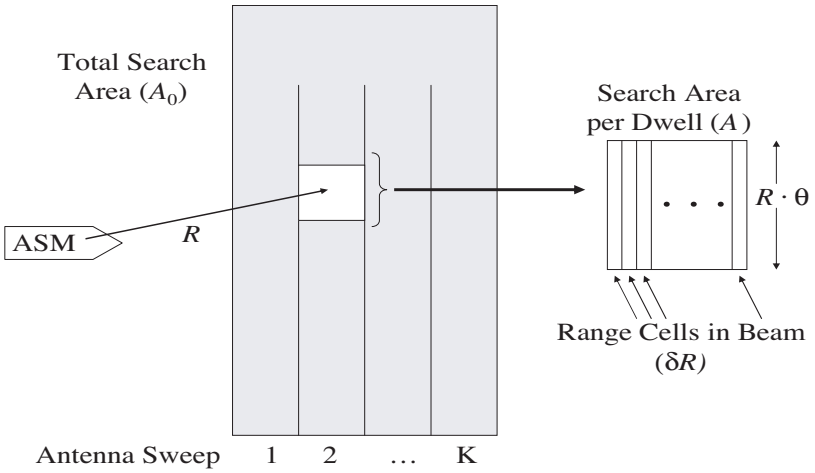

Fig. 3 — ASM search area

The Doppler processing for each dwell area is accomplished by matched-filtering over the P pulses and the CPI is

$$CPI = P \cdot PRI. \tag{3}$$

{Note on the PRF: The maximum unambiguous range is related to the inverse PRF as

$$R_{\max} = c/(2 \cdot PRF). \tag{4}$$

Thus, at shorter ranges, a higher PRF may be used. Similarly, the magnitude of the maximum unambiguous radial speed is related to PRF as

$$V_{\max} \cdot 2 = PRF \cdot (\lambda/2). \tag{5}$$

Thus, if the PRF is increased, there may be Doppler cells that would not contain targets.}

It is assumed that the PRF is the same for both seeker systems and that the PRF is such that there are no range or Doppler ambiguities. The number of independent Doppler cells investigated over the CPI is P. If we assume that the PRF is such that all of the cells correspond to possible target speeds, then N_D equals P and

$$N_I = N_C. \tag{6}$$

Under these assumptions, the probability of false alarm in any particular location in detection space is the same for both seekers. Note that a detection space location is the geometric location (range and angle) at a particular time (pulse) for the noncoherent seeker and that it is the geometric location (range and angle) and radial speed (Doppler) at a particular time (CPI) for the coherent seeker.

Search Mode Analysis—Probability of Detection

Next, assume that the target return is expected to obey the same statistics for both cases, e.g., a fluctuating (Swerling) target and a square-law detector. If the performance criteria relates a required probability of detection for the stipulated false alarm rate, then, since the detection cell probability of false alarm is the

same, the performance criteria relates to the same required (or threshold) signal-to-noise ratio (SNR) for the seekers, i.e., the required SNR per PRI (noncoherent seeker) equals the required SNR per CPI (coherent seeker).

Using standard notation, the general expression (valid for both seekers) is given for the radar range equation in terms of the coherent processing time, the various losses, and the system noise:

$$SNR = [(P_{avg} \cdot G^2 \cdot \lambda^2 \cdot \sigma \cdot T_{coh})] / [\{4\pi\}^3 \cdot (L \cdot kT \cdot F \cdot R^4)]. \tag{7}$$

Search Mode—Performance Analysis

The common terms between the implementations relate to the antenna, carrier frequency, and internal parameters such as system noise and losses. Obviously, these terms vary from implementation to implementation, depending on the integrity of the implementation and components used. They are assumed equal for this analysis. The next two expressions are for the particular subject seekers. In each case, the SNR is written to isolate the assumed common terms. For the coherent seeker, the CPI has been set equal to $P \cdot PRI$, as above. For the noncoherent seeker, the processing time has been set equal to the pulse interval (PRI) and the systems have the same PRF (or PRI).

$$SNR_C = \{[(G^2 \cdot \lambda^2)] / [(4\pi)^3 \cdot (L \cdot k \cdot T \cdot F)]\} \cdot [(P_{avg_C} \cdot \sigma_C \cdot P \cdot PRI) / R_C^4], \tag{8}$$

$$SNR_I = \{[(G^2 \cdot \lambda^2)] / [(4\pi)^3 \cdot (L \cdot k \cdot T \cdot F)]\} \cdot [(P_{avg_I} \cdot \sigma_I \cdot PRI) / R_I^4]. \tag{9}$$

To compare noncoherent and coherent phenomenology, these expressions are set equal, or

$$(P_{avg_C} \cdot \sigma_C \cdot P) / R_C^4 = (P_{avg_I} \cdot \sigma_I) / R_I^4. \tag{10}$$

Search Mode Performance Analysis—Equal Average Power Assumption

It was previously assumed that both systems have the same PRF (or equivalently, PRI) and the same range resolution. To compare target detection capabilities, it is now assumed that both systems transmit the same average power. Again, there are many variables and much variation in the technologies required to implement a radar seeker. However, a general rule is that the cost of a radar system relates to transmitter cost and transmitter cost relates to average power. Or, saying it another way, the system cost increases with higher peak power and/or higher duty cycle. Setting the average powers equal in the above result gives

$$(\sigma_C \cdot P) / R_C^4 = (\sigma_I) / R_I^4. \tag{11}$$

Thus, for equal SNR, the ratio of the detectable target scattering cross section over the fourth power of the range for the two systems relates to the number of pulses added in the CPI. Figure 4 shows simple illustrative results. It was assumed that 16 pulses are integrated for the Doppler processing and that the noncoherent seeker could detect a 40 dBsm target at 20 km. For this case, the important point is that the coherent seeker has comparable performance for targets smaller by 12 dB at a given range or comparable performance for the same target at twice the range.

This analysis compares the range and target size thresholds for equal seeker performance (FAR and probability of detection). The same analysis can be used to compare the seeker performance for a given target at a particular range. For the given example, the coherent system would process a given target signal at a particular range at a SNR that is 12 dB greater. This translates into a higher probability of detection and more accurate parameter measurements.

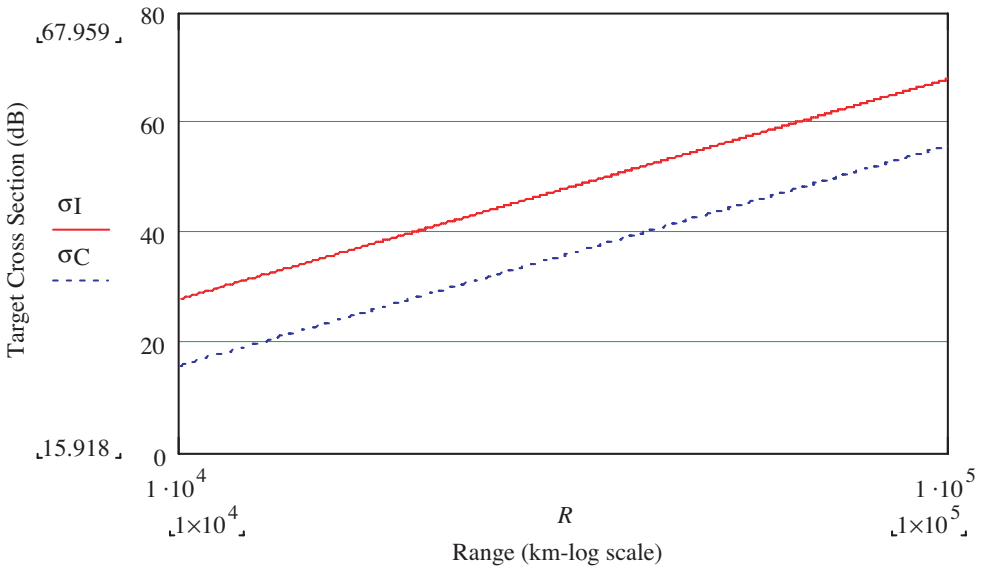

Fig. 4 — Target cross section at threshold of detection capability vs range

Search Mode Performance Analysis—Peak Power

Various assumptions have been made up to this point. In particular, the two systems are assumed to have the same PRF, the same range resolution, and the same transmitted average power. Thus, it has been assumed that the product of peak pulse power and pulsewidth is equal, or

$$P_{pk_C} \cdot PW_C = P_{pk_I} \cdot PW_I. \tag{12}$$

The previous results are valid as long as the products, as shown, are equal.

There may be several reasons to prefer to not set these individual parameters equal. It is somewhat easier to maintain coherence through the various system components if the peak power is lower. The transmitter power sources tend to be more efficient at higher duty cycles. Also, coherence is easier to maintain with longer pulses, with some pulse shaping to avoid sharp edges on the pulse. Thus, a lower peak power can be used on a longer pulse to maintain the same average power for target detection. To maintain the same range resolution (as assumed thus far), intrapulse modulation can be implemented to match the pulse bandwidth of the noncoherent seeker. In addition to all of the above reasons, the seeker emissions are then expected to be more difficult to intercept via ES. This strategy maintains comparable target detection performance with added LPI capabilities.

Continuing the example above, it is assumed that the noncoherent radar pulsewidth (PW) was 0.125 μs. The same range resolution can be achieved for the coherent seeker by maintaining the same bandwidth through intrapulse modulation. For example, assume that the coherent seeker pulse bandwidth (BW) is 8 MHz and the PW_C is 8 μs. For the parameters assumed, a coherent seeker with a peak power of 600 W (28 dBw) has detection performance corresponding to that of the noncoherent radar with a peak power of 38 kW (46 dBw). For these parameters, the coherent seeker peak power is 64 times (about 18 dB) less than that of the noncoherent radar.

Search Mode Performance Analysis—Clutter

The analysis to this point has assumed that the noise of interest is white noise. In particular, white noise distributes evenly in Doppler. Sea clutter presents another and very significant interference or colored noise

background to the processor. Doppler is generally thought of as a measure of the target's radial speed relative to the ASM. Normally, the processing shifts the Doppler of the main clutter to be at zero Doppler. Thus, measured Doppler of a reflector's return is its closing radial speed relative to the center of the mainbeam clutter. Since the ASM radial speed contribution varies with look angle, the Doppler of a return varies with angle within the beam. In this sense, the Doppler measurement can be considered to be a combination of target radial speed and angle within the beam (Fig. 5). (This is discussed in more detail below.)

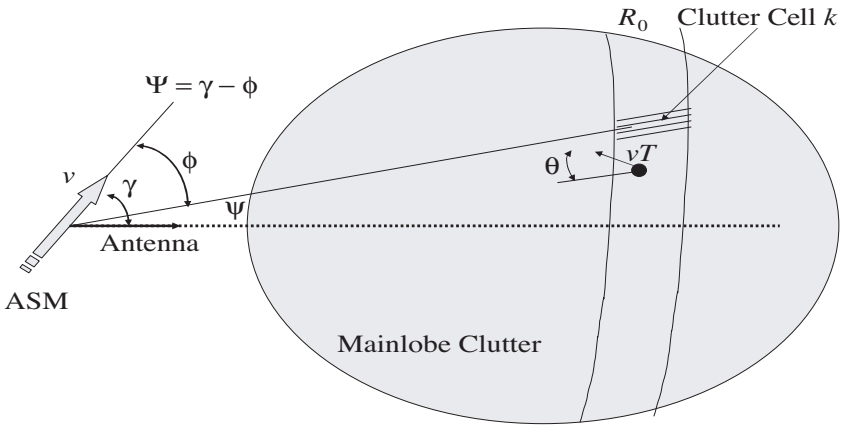

Fig. 5 — Clutter geometry

Any return levels are weighted by antenna gain at the source position within the beam through the angular dependence in the factor G^2 in the range equation expression above. Since the ASM processing centers the mainbeam clutter at zero Doppler, the interference pattern resembles that shown in Fig. 6. There is a noise floor from the aliasing of the sidelobe clutter (SLC) returns, and there is the larger mainlobe clutter (MLC) centered on DC (the 0 Hz Doppler cell). As indicated in the figure, the MLC broadens (vs Doppler frequency) and decreases in peak amplitude at DC as the angle increases between the ASM velocity and the antenna. (For use below, it is noted that the perceived broadening of MLC is a result of the relationship between the ASM parameters and measured Doppler of the components of the sea clutter.)

The SLC is composed of about 15 dB greater sea surface area than that of MLC, but it is spread over about 16 Doppler cells for the present example. This reduces the clutter per cell by 15 dB. The SLC levels are down at least another 30 dB because of the reduced antenna gain. Thus, it is expected that the SLC floor is about 30 dB or more below the MLC level and is therefore neglected.

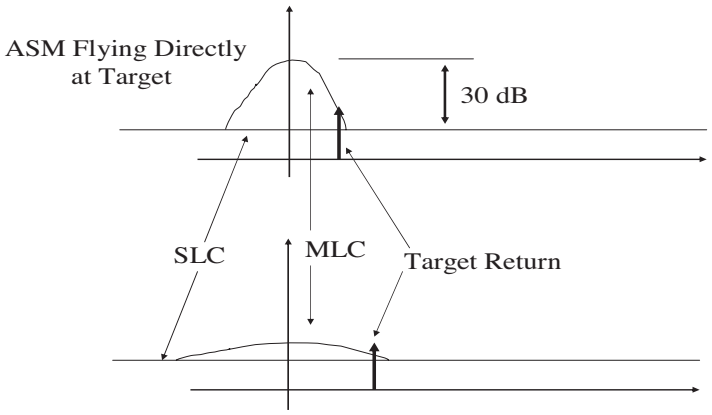

Fig. 6 — Doppler spectra

The radar cross section for sea clutter at low grazing angle can be estimated by assuming a scattering coefficient of –35 dB/area. Using a beamwidth of 8 deg, a range of 20 km, and a range resolution of about 20 m (area equals 47 dB), the clutter scatter cross section for MLC is 12 dB. For more coarse range resolution, the clutter cross section is proportionally larger. (Note, as shown below, that the clutter-to-noise ratio (CNR) varies as R^{-3} while the signal-to-clutter ratio (SCR) varies as R^{-1}.)

At multiples of Mach 1 and at a look angle of 5 deg or more, it is expected that the MLC significantly spreads over multiple Doppler cells. Thus, the interference level may be about the same as that of a small target of radar cross section of 0 to 20 dB in particular (low) Doppler cells. Although this is still much smaller than a standard ship target, it indicates that the detection problem may be clutter-limited in the low Doppler cells and at shorter ranges as opposed to being noise-limited in the higher Doppler cells at all ranges.

As in the discussion above for SNR and using a standard, simple model, the comparable expressions for CNR are (where the A's represent the clutter surface areas)

$$CNR_C = \{[(G^2 \cdot \lambda^2)] \; / \; [(4\pi)^3 \cdot (L \cdot k \cdot T \cdot F)]\} \cdot [(P_{avg_C} \cdot \sigma_0 \cdot A_C \cdot P \cdot PRI) / R_C^4], \tag{13}$$

$$CNR_I = \{[(G^2 \cdot \lambda^2)] \; / \; [(4\pi)^3 \cdot (L \cdot k \cdot T \cdot F)]\} \cdot [(P_{avg_I} \cdot \sigma_0 \cdot A_I \cdot P \cdot PRI) / R_I^4]. \tag{14}$$

Computing the SCR's gives

$$SCR_C = \sigma_T / (\sigma_0 \cdot A_C), \tag{15}$$

$$SCR_I = \sigma_T / (\sigma_0 \cdot A_I). \tag{16}$$

Thus, if the areas (antenna beamwidth, range, and range resolution) are the same, the SCR of the coherent system in the low Doppler cells is the same as the SCR of the noncoherent system. Again, the coherent system retains a significant detection advantage for targets at nonzero radial speeds and for targets that are not at the center of the antenna beam. But the coherent system does not have a detection advantage for targets at low Doppler if both systems have the same range resolution.

Obviously clutter spikes are a special case. Clutter spikes can have significant cross section and significant nonzero relative Doppler. Thus, clutter spikes can appear similar to low cross section targets when viewed with a coherent seeker that does not have significant imaging capability.

Target Discrimination

Target discrimination is a critical capability for the ASM seeker, especially in the presence of jamming and other EA (Electronic Attack). For this analysis, it is only indicated that the coherent seeker presents more information at, perhaps higher resolution, to the postprocessor for discrimination purposes.

Track Mode Performance Analysis

Beyond detection performance, the seeker may be required to provide inputs to the guidance system. The critical guidance parameters are, first, angle off boresight and, second, time to go. For this analysis, it is only commented that the parameter measurement accuracy is generally proportional to inverse SNR or SCR. Thus, the results above can be applied to this issue.

Electronic Protection Analysis

Several obvious EP advantages might be available to the coherent seeker, as defined thus far, that are mentioned at this point. It was previously indicated that the addition of intrapulse modulation is expected to make the seeker more difficult to monitor and detect (LPI). Also, various standard processing techniques may be used to resolve a decoy from the target, such as versions of beat frequency detection (BFD) and Doppler beam sharpening (DBS). In addition, Space-Time Adaptive Processing (STAP) can be implemented to improve resolution and detection of targets with low radial velocity. These techniques are discussed in the references.

Summary

With the chosen parameters (Table 2) the noise-limited detection range is 9.4 km with the noncoherent seeker and twice that (18.7 km) with the two coherent seekers. Also, the peak power is lower with the second (wide pulse) coherent seeker. The primary purpose has been to examine the attributes of the seeker when coherence is added to the radar capabilities. In the next section, the comparison analysis is repeated for what are expected to be more realistic parameters for two different seeker radars (noncoherent and coherent).

Table 2 — Systems Comparison Summary

Parameter	Noncoherent	Coherent-1	Coherent-2
FAR	1/h	1/h	1/h
PFA/cell	$4.6 \cdot 10^{-10}$	$4.6 \cdot 10^{-10}$	$4.6 \cdot 10^{-10}$
PD	0.5	0.5	0.5
SNR (required)	14.8 dB	14.8 dB	14.8 dB
Range swath	6 km	6 km	6 km
λ	X-band	X-band	X-band
P_{pk}	1 kW	1 kW	15.6 W
PRF	2 kHz	2 kHz	2 kHz
PW	0.125 μs	0.125 μs	8 μs
P_{avg}	0.25 W	0.25 W	0.25 W
G	25 dB	25 dB	25 dB
Bandwidth	8 MHz	8 MHz	8 MHz
δR	20 m	20 m	20 m
Beamwidth	8 deg	8 deg	8 deg
Pulses/CPI	—	16	16
F	3 dB	3 dB	3 dB
L	10 dB	10 dB	10 dB
σ_T	35 dBsm	35 dBsm	35 dBsm
Noise-limited range	9.4 km	18.7 km	18.7 km
Clutter (–35 dB) at 20 km	12.5 dB	12.5 dB	12.5 dB

For this example, the results are summarized in Fig. 7. The upper curve shows the signal-to-interference for the coherent radar in Doppler cells away from DC (nonzero radial speed). The SNR varies as R^{-4}. The middle curve shows the results for the Doppler cells corresponding to the low radial speeds. At long range, the performance is noise-limited. At shorter range, the performance becomes clutter-limited. The lower curve shows the results for the noncoherent example. Again the performance is noise-limited at long range, where

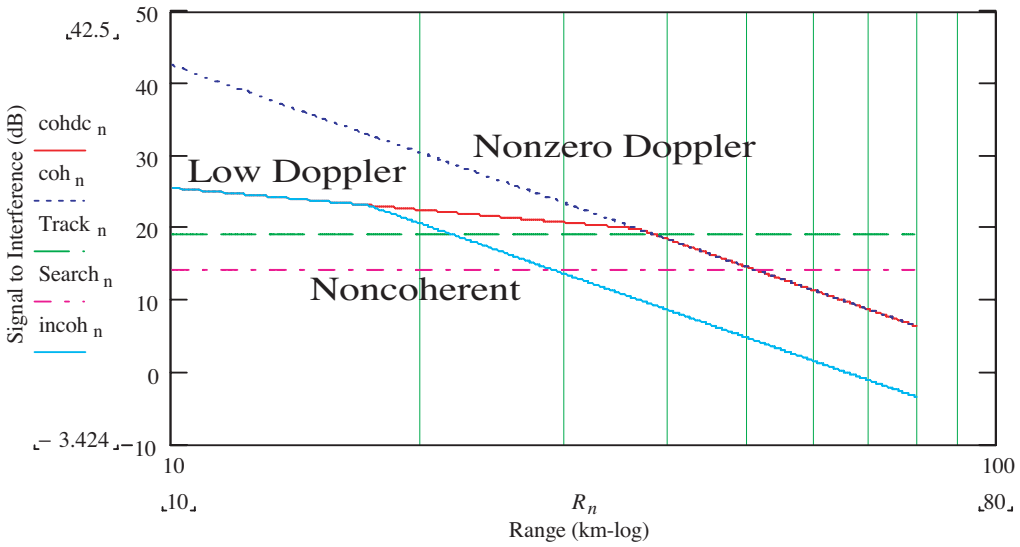

Fig. 7 — Signal-to-interference ratio vs range

the gain resulting from coherent integration gives the coherent seeker a performance advantage. Within the clutter-limited region, there is no significant performance difference between the implementations for Doppler cells containing MLC when the systems have the same range resolution. The threshold lines for track and search probabilities of detection (0.8 and 0.5, respectively) are also shown.

To view the result in another way, when the noncoherent seeker processes a detection cell, all of the noise associated with that cell limits the detection performance. When the coherent seeker views the same detection cell over multiple pulses, the target energy adds coherently while the noise energy adds incoherently. In addition, the energy spectrum is sorted into separate frequency bands, further reducing the noise per cell. Figure 8 illustrates this effect.

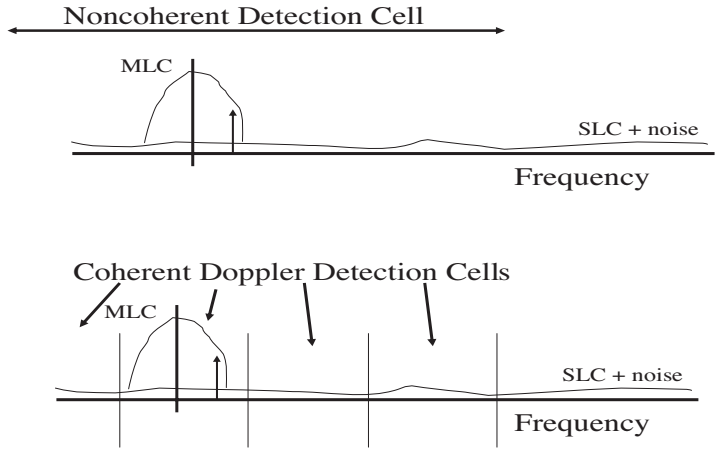

Fig. 8 — Spectral separation of noise

In addition to the parameters listed, during this analysis it has been assumed that the target is equally likely to occur in any detection cell including all of the Doppler cells. No postdetection integration has been assumed, i.e., a single look per cell. It has been assumed that the detection statistics are the same for each case. It has been assumed that each system has the same average power and the same range resolution. In

particular, it has been assumed that the coherent radar Doppler cells contain no clutter (nonzero cells) or all of the clutter (labeled "Low Doppler").

REALISTIC SYSTEMS—ANALYSIS AND DISCUSSION

Second Comparison

In this section, different assumptions are made in comparing the systems. As in the previous section, assume that the required probability of detection is 0.5 in search mode and 0.8 in track mode, with a corresponding false alarm rate (FAR) of 1 per hour. Assume the X-band radar system descriptors (both independent and dependent) as listed in Table 3. From the assumed system parameters, the range resolution and number of range gates per swath are computed. From this information, the probability of false alarm per detection cell is computed. This PFA/cell and assuming Swerling II target statistics implies the detection threshold. This information, together with the required detection probability, implies the required SNR for each case. In this section, it is assumed that the target of interest has a radar cross section (σ_T) of 35 dBsm and the SIR observed is computed as a function of range. (Again, the overall system noise figure and system loss have been assumed equal.)

Table 3 — Realistic System Descriptors

Variable	Noncoherent	Coherent
Range swath	3 km	3 km
λ	X-band	X-band
P_{pk}	35 kW	200 W
PRF	2 kHz	2 kHz
PW	1 μs	20 μs
P_{avg}	70 W	8 W
G	25 dB	25 dB
Bandwidth	1 MHz	10 MHz
δR	150 m	15 m
Beamwidth	8 deg	8 deg
Pulses/CPI	—	16
F	3 dB	3 dB
L	10 dB	10 dB

As before, the SNR can be computed vs range as

$$SNR = [P_{avg} \cdot G^2 \cdot \lambda^2 \cdot T_{coh} \cdot \sigma_T] / [(4\pi)^3 \cdot L \cdot kT_0 \cdot F \cdot R^4]. \quad (17)$$

Assuming the simple clutter model, the clutter interference must also be computed to determine if the target detection is clutter-limited, i.e., if the clutter is larger than the noise or, similarly, if the signal-to-clutter ratio (SCR) is less than the SNR. It is assumed that the sea clutter scatter coefficient (σ_0) is –35 dB and the clutter is the clutter coefficient times the pulse area on the sea. Thus, at low grazing angles, the SCR is

$$SCR = \sigma_T / [\sigma_0 \cdot \delta R \cdot \theta \cdot R]. \quad (18)$$

Table 4 summarizes the results. For this example, Fig. 9 also summarizes the results. As before, the upper curve shows the signal-to-interference for the coherent radar in Doppler cells away from DC (zero

Table 4 — Performance Results Summary

Variable	Noncoherent	Coherent
FAR	1/h	1/h
PFA/cell	$3.5 \cdot 10^{-8}$	$3.5 \cdot 10^{-10}$
Threshold	12.3 dB	13.4 dB
Search Mode Results		
PD	0.5	0.5
SNR (0.5)	14.2 dB	14.1 dB
Noise-limited range	39.6 km	46.2 km
Track Mode Results		
PD	0.8	0.8
SNR (0.8)	19.2 dB	19.1 dB
Noise-limited range	29.7 km	34.7 km
Clutter		
SCR (at 20 km)	13.8 dB	23.8 dB
SCR (at 30 km)	12.0 dB	22.0 dB

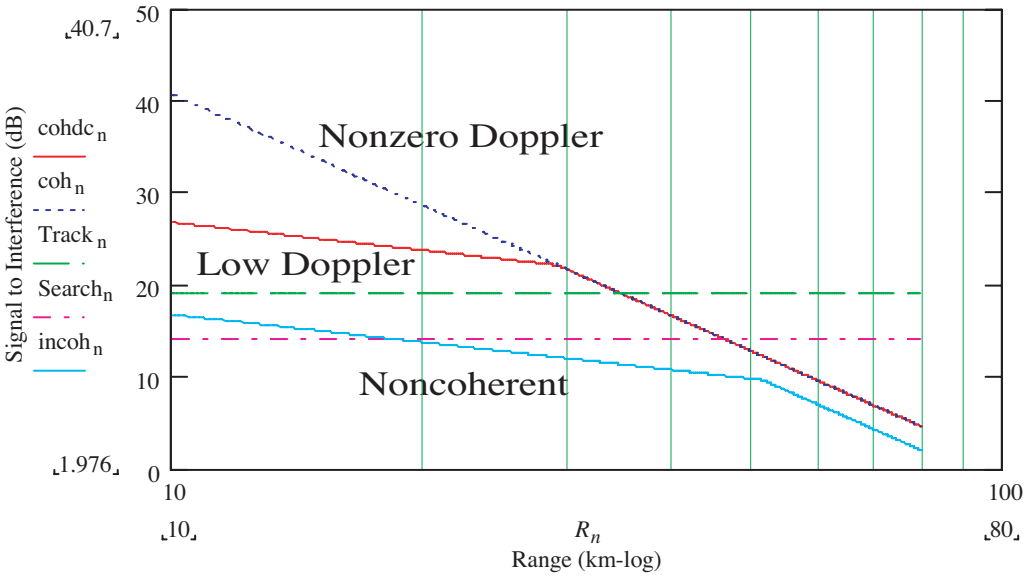

Fig. 9 — Signal-to-interference ratio vs range

radial speed). The next curve shows the results for the Doppler cells corresponding to the low radial speeds. The lower curve shows the results for the noncoherent example. The threshold lines for track and search probabilities of detection are also shown.

The results are similar to those shown in Fig. 7. The improvement of the coherent example in the noise-limited region results from the assumption of interpulse coherent integration (CPI vs PRI). [Note: The improvement in the noise-limited region is mitigated relative to the previous case by the significant difference in average power of 9.4 dB.] In this comparison, there is a 10 dB performance advantage in the clutter-limited region resulting from the finer range resolution or the use of intrapulse coherent integration.

Figure 10 illustrates the performance improvement in the clutter-limited region that results from range compression. As shown, the target energy is assumed to still be contained within a detection cell. However, the amount of clutter noise in a detection cell is reduced by an amount directly related to the finer range resolution.

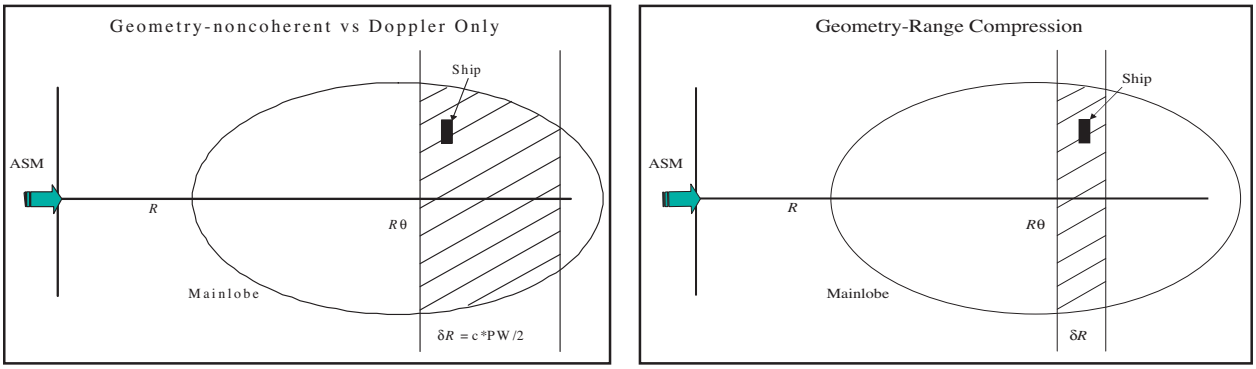

Fig. 10 — Performance improvement in clutter due to range compression

Doppler Beam Sharpening Phenomenon

The results illustrated in Fig. 9 assume that all of the MLC (for the coherent radar) resides within the lowest (the 0 Hz frequency) Doppler cell. That is, the area of the clutter patch within the 0 Hz Doppler cell, with θ representing the beamwidth, is

$$A = R \cdot \mathrm{d}R \cdot \theta. \tag{19}$$

In reality, the cross range dimension of a single Doppler cell can be represented as approximately R times $\delta\psi$, as indicated in Fig. 5.

If the cell is sharpened in this manner and if the target is in this clutter cell, the SCR increases with ASM high speed (v) and maneuvers (γ):

$$SCR = [\sigma_T/(\sigma_0 \cdot \delta R \cdot R \cdot \delta\psi)]. \tag{20}$$

Figure 11 illustrates this effect. For the parameters listed above and at Mach 1 at a 5-deg look angle, the coherent SINR is improved by 3 dB in the clutter-limited region. If the ASM flies at Mach 3, the improvement is about 7 dB. Figure 12 shows this result.

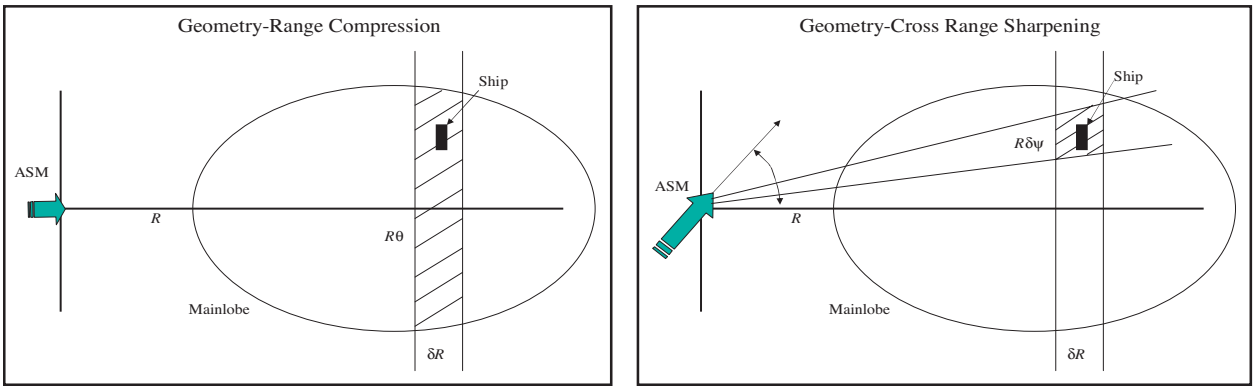

Fig. 11 — Clutter reduction resulting from beam sharpening

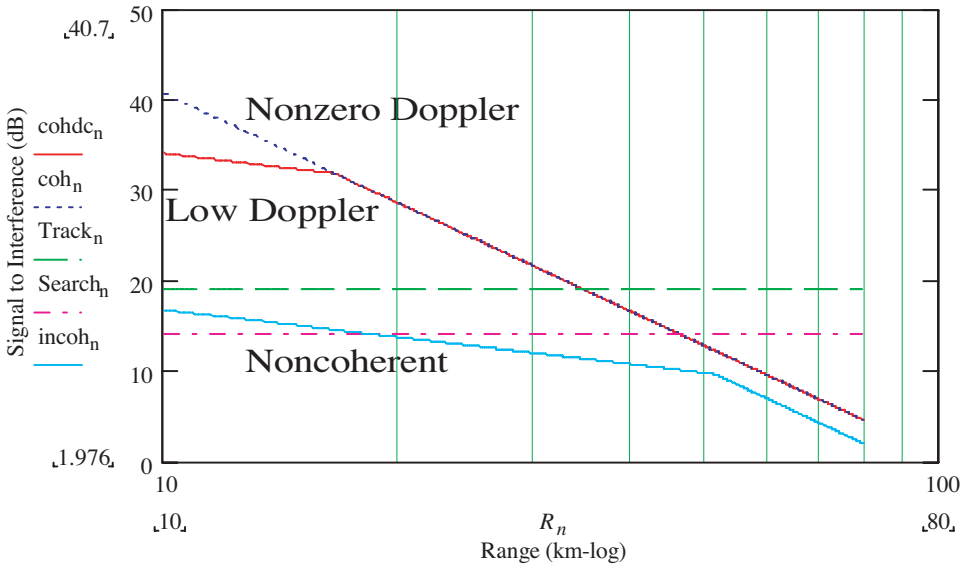

Fig. 12 — Signal-to-interference vs range

Summary

In this section, more realistic parameters were chosen, and the expected performance of the ASM non-coherent seeker is compared with that of an ASM coherent seeker. As before, the objective is to highlight some of the potential advantages associated with the addition of interpulse and/or intrapulse radar coherence and to provide a simple understanding of the cause of this gain.

The coherent system can use much lower peak power and a wide pulse to improve EP capabilities. At the same time, added discrimination capability is available, and the coherent system is expected to have improved detection range and guidance measurements accuracies.

Also, the performance in the clutter region may be further improved if the coherent radar guided ASM can sharpen the azimuth resolution via maneuvers (looking off the nose) and/or higher speed. These tactics have other advantages for the ASM in addition to those discussed.

Again reviewing the analysis leading to the results summarized in Fig. 9, in addition to the parameters listed it has been assumed that the target is equally likely to occur in any detection cell including all of the

Doppler cells. No postdetection integration has been assumed, i.e., a single look per cell. It has been assumed that the detection statistics are the same for each case. In particular, it has been assumed that the coherent radar Doppler cells contain no clutter (nonzero cells) or all of the clutter (labeled "Low Doppler"). However, it has been assumed that the low Doppler cell of interest has been narrowed or sharpened.

PROCESSING IN CLUTTER

Background

The ultimate goal of the antiship missile seeker is to generate adequate target range and angle estimate inputs to the guidance system to enable the ASM to impact the ship. Signal processing is applied to the data to better detect the ship return and to extract the measurements. Examples of this signal processing include range compression, Doppler processing, detection, target discrimination, and monopulse angle estimation. A relevant question is whether this processing is optimal in the sense of providing adequate detection and parameter estimates to successfully fulfill the mission requirements. This section addresses particular aspects of the Doppler and monopulse processing in a coherent radar seeker. This analysis is intended to serve as the basis for a more in-depth analysis.

To extract the measurements for the guidance algorithm requires reliable detection (high probability of detection at low probability of false alarm) at significant SNR. One reason to use the coherent radar seeker is to improve the SNR. The SNR can be improved by coherent Doppler processing gain, by using finer range cells, and by separating the target return from the clutter returns and other interference through the Doppler processing. Higher SNR improves both target detection and measurement accuracy:

$$\textit{Measurement Variance} = k/SNR. \tag{21}$$

The clutter is concentrated in the lower Doppler cells since the coherent seeker (CS) processing is designed to center the ASM motion-induced Doppler of the clutter on the 0 Hz Doppler cell. It is expected that the probability of detection of ships for the CS will be adequate for targets with significant Doppler. If the ASM approaches the target on broadside, then the target Doppler is lower, but the cross section is larger.

In general, but especially when the ASM maneuvers (and during Search mode), the angle between the ASM velocity and its antenna is nonzero. It was shown previously that the MLC spreads across multiple Doppler cells from the zero-cell as this look angle increases. A nonzero angle between the velocity and the antenna corresponds to a lower peak clutter level within the low-frequency Doppler cells, while MLC spreads to higher Doppler values. The sidelobe clutter (SLC) varies over many kHz. For typical ASM processing parameters, this low-level SLC return is expected to wrap over the entire Doppler spectrum as a result of significant spectral aliasing.

As discussed above and in the Appendixes, the estimate of the target Doppler from the CS contains an additive component resulting from the nonzero pointing angle with the CS velocity (angle γ; see Fig. 5 and the Appendixes) and from nonzero (relative to the target direction) offset of the antenna pointing angle (angle ψ). Thus, it is possible that the target detection and tracking parameters (Doppler and pointing angle from boresight) estimates are corrupted by clutter, especially at low ship radial velocity. Intentional jamming may also corrupt the target detection and parameter values.

To summarize, clutter and/or intentional interference or jamming can decrease the ship detection probability and can degrade the parameter estimates required for ASM guidance. Improved understanding of the CS received signals can be used to evaluate and, if necessary, minimize these errors. This section examines a representation for the received signals that can be used to further investigate the CS performance. In ad-

dition, STAP (Space-Time Adaptive Processing) is briefly reviewed as an indication of standard processing that can be used to mitigate these effects. STAP processing has the advantage of adapting to the clutter (and possible jamming) interference for improved detection of targets at low Doppler and, subsequently, improved parameter estimation accuracy.

Purpose

This section addresses the processing representation that can be used to improve the detection and to improve the guidance parameter estimates of targets at low Doppler given monopulse capability together with the previously discussed coherent radar.

Discussion of Analysis

The Appendixes contain an analysis of the received signals for the sum and delta channels for the purpose of generating a representation of the received signals. It is assumed that P pulses in a single coherent processing interval (CPI) are collected prior to Doppler processing. The received signals at a particular range cell for pulse p are represented as in Eqs. (A20) and (A21) (using Eqs. (A24) and (A25)):

$$\Sigma_p = a \cdot \exp\left[2\pi i(\beta\Phi_T + \alpha_T)p\right] \cdot \cos\left(2\pi\Phi_T\right) + \Sigma_k \left[c_k \exp\left[2\pi i\ (\beta\Phi_k)p\right] \cos\left(2\pi\Phi_k\right)\right] + n_p, \tag{22}$$

$$i\Delta_p = a \cdot \exp\left[2\pi i(\beta\Phi_T + \alpha_T)p\right] \cdot \sin\left(2\pi\Phi_T\right) + \Sigma_k \left[c'_k \exp\left[2\pi i\ (\beta\Phi_k)p\right] \sin\left(2\pi\Phi_k\right)\right] + n'_p. \tag{23}$$

The a represents the amplitude of the target, the c_k's represent clutter component amplitudes, and n (and n') represents the noise terms. (Note that jamming interference can be easily incorporated into this general representation.) These two signals can be combined (sum and difference) to form a $2P$ dimensional vector for the CPI and range cell of interest, as shown in Eq. (A27) (see Eqs. (A22) and (A23)):

$$X = a \cdot X_T + X_c, \tag{24}$$

where X_T represents the Doppler-pointing angle steering vector (target matched-filter) and X_c represents the interference (clutter and/or jamming) plus noise. The components of the individual vectors are of the form

$$X_T = \{\exp\left[2\pi i(\beta\Phi_T + \alpha_T)p\right] \cdot \exp\left(+2\pi i\Phi_T\right)\} \text{ or } \{\exp\left[2\pi i(\beta\Phi_T + \alpha_T)p\right] \cdot \exp\left(-2\pi i\Phi_T\right)\} \tag{25}$$

$$X_c = \{\Sigma_k \left[c_k \exp\left[2\pi i\ (\beta\Phi_k)p\right] \exp\left(+2\pi i\Phi_k\right)\right] + N_p\}, \tag{26}$$

or

$$\{\Sigma_k \left[c_k \exp\left[2\pi i\ (\beta\Phi_k)p\right] \exp\left(-2\pi i\Phi_k\right)\right] + N'_p\}. \tag{27}$$

From the expressions above, the standard estimate of target Doppler (via the fast Fourier transform (FFT)) contains the additive effect of the ASM motion and any antenna-offset angles (imbedded in the definitions of β and Φ_T). This result was mentioned in Ref. 7. That is, the target Doppler occurs at

$$\alpha = \alpha_T + \beta\Phi_T. \tag{28}$$

However, the input to the Guidance Algorithm extracted from monopulse processing (or the equivalent matched-filter processing, Φ_T) will be correct, but only if the clutter and jamming (nonwhite interference) can be neglected.

General X_c

For the case of a general X_c, both the detection of the target and the subsequent estimates of the tracking parameters are degraded. This is especially true when significant clutter and/or jamming is present. To assess the degree of degradation requires a more detailed analysis of the specific situation than presented herein. For this case, prewhitened matched-filter processing provides both the optimal detector and the optimal parameter (Doppler and pointing angle) estimator.

The detection and/or estimation problem can be formulated in terms of the output (z) of the signal processing that is a linear combination of the CPI data,

$$z = W^{+} \cdot X. \tag{29}$$

The scalar output of the processing is indicated above where the Hermitian conjugation (complex conjugate and transpose) operation is indicated on the weighting vector **W**. The signal-to-interference and noise ratio is

$$SINR = [a^2 \cdot (W^{+} \cdot X_T) \cdot (X_T^{+} \cdot W)] / [W^{+} \cdot M \cdot W] < a^2 \cdot X_T^{+} \cdot M^{-1} \cdot X_T, \tag{30}$$

where M is defined in Appendix A (Eq. (A30)) and Cauchy's inequality was used in the last step. Equality (maximum SINR) to the Cauchy upper bound is achieved for the optimal weighting vector as shown in Appendix A,

$$W_{opt} = M^{-1} \cdot X_T. \tag{31}$$

Thus, the optimal processing is the prewhitened matched-filter. In general, M is unknown and must be estimated resulting in suboptimal processing. In the absence of a priori knowledge of the optimal filter, various STAP processing schemes have been developed to provide estimates of the filter. Basically, the goal of STAP is to adapt to the background noise for the purpose of prewhitening the noise prior to the matched-filter. The effect of STAP is to reduce the region where processing is degraded in the manner of classical MTI filtering. (Note: classical MTI filtering can be shown to be equivalent to STAP with additional assumptions; see Ref. 1, Section 5.2.1.)

Additive White Noise, or $X_c = N$

This assumption neglects the clutter and jamming. It assumes additive white noise with variance σ^2 or $M = \sigma^2 \cdot I$. If the interference can be represented as additive white noise, then

$$W_{opt} = \sigma^{-2} \cdot X_T. \tag{32}$$

In this case, the processing can be expressed in terms of the search over Doppler-pointing angle space X_H where X_H is the unknown, hypothesized steering vector. Or, in general,

$$W = \sigma^{-2} \cdot X_H \qquad \text{for all } X_H = \{\exp[2\pi i(\beta\Phi + \alpha)p] \cdot \exp(\pm 2\pi i\Phi)\}, \tag{33}$$

$$SINR(\alpha, \Phi) = 2P \cdot (a/\sigma)^2 \cdot \operatorname{sinc}[\pi \cdot P \cdot (\alpha_T + \beta \cdot \Phi_T - \alpha)] \cdot \cos[2\pi \cdot (\Phi - \Phi_T)], \tag{34}$$

$$SINR_{\max} = 2P \cdot (a/\sigma)^2 \qquad \text{at } X_H = X_T. \tag{35}$$

In this case, a simple manipulation of the output expression for z shows that, processing with W proportional to the steering vector (X_H) in unknown Doppler and pointing-angle is equivalent to the two-staged processing of Doppler (DFT) followed by angle estimation. Again, the standard estimate of target Doppler contains the additive effect of the ASM motion and any antenna-offset angles. That is, the peak in Doppler occurs at

$$\alpha = \alpha_T + \beta \cdot \Phi_T. \tag{36}$$

However, the input to the Navigation Algorithm extracted from monopulse processing (or the equivalent matched-filter processing, Φ_T) will be unbiased.

Summary and Conclusion

A general model representation for the processed (through the range processing and analog-to-digital processing) CS signals is derived and presented in Appendix A. The model incorporates arbitrary geometry and various targets including ships, clutter, and jamming. STAP processing is briefly reviewed and summarized. The optimal processing for the CS is shown to be an adaptation of STAP for the case of an antenna consisting of two elements or subarrays (monopulse). Standard Doppler processing followed by monopulse angle estimation is equivalent to the optimal processing (STAP) when the interference is equivalent to additive white noise. In general, the estimate of target Doppler is corrupted by CS motion and antenna offset angle, but the angle estimate inputs to the guidance system are unbiased if the distortions resulting from clutter and/or jamming interference can be neglected.

Figure 13 illustrates the typical flow of combined Doppler and monopulse processing. The output of the RF processing from both the Σ and Δ channels for a CPI are combined as previously discussed to form a $2P$ dimensional vector at each range cell. The vector components are weighted and linearly combined with the estimate of W. The estimation procedure uses the data as in the many versions of STAP theory. This process results in an array of amplitudes as a function of range, look angle, and Doppler. This array is then processed for detection and parameter estimation using standard signal processing. Thus, the unique aspect of this approach is to combine and process the CPI data with an estimate of the prewhitening filter as opposed to Doppler filtering and then monopulse estimation for the purpose of mitigating clutter and possible jamming.

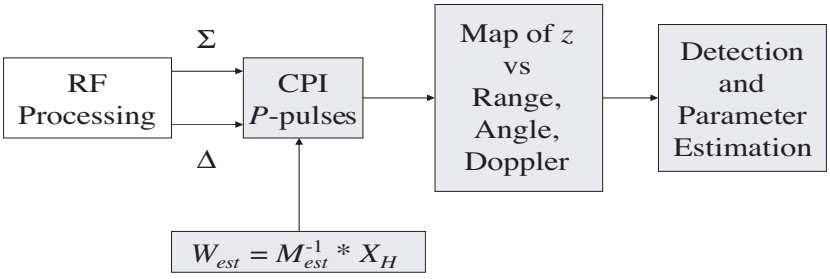

Fig. 13 — Combined Doppler/monopulse processing

SUMMARY AND RECOMMENDATION

An investigation was conducted of potential processing advantages to the guidance of ASM via coherent radar. In the first case, the coherent radar case was compared with an identical noncoherent ASM except for the addition of Doppler processing. It was seen that Doppler processing provided improved performance proportional to the number of pulses integrated in the noise-limited regions. However, there was no gain in the clutter-limited region (shorter ranges) for targets within the MLC, that is, targets with minimal radial speed relative to the ASM.

Next, it was shown that improved range resolution (for example, via range compression) translated directly to improved performance in the clutter-limited region. Another case was analyzed in which the two ASM systems (guided via noncoherent and guided via coherent radar) had more realistic technical capabilities. The results were similar to the prior results. Doppler processing provided improved performance in the noise-limited situations and range compression provided improved performance in the clutter-limited situations.

Finally several techniques were investigated that improved performance in the clutter-limited region. The first technique is Doppler sharpening of the cross-range resolution. The second technique investigated is the use of coherent processing combined with monopulse capability to provide clutter mitigation processing capability analogous to STAP (ΣΔ-STAP).

It is recommended that the analysis be applied to specific ASM and seeker parameters. If it is determined that clutter or jamming mitigation is required, the techniques suggested should be investigated further.

BIBLIOGRAPHIES

1. J.R. Guerci, *Space-Time Adaptive Processing for Radar* (Artech House, Norwood, MA, 2003).

2. "Space Time Adaptive Processing," C & P Technologies, Inc., at www.cptnj.com.

3. G. Morris and L. Harkness, *Airborne Pulsed Doppler Radar* (Artech House, Norwood, MA, 1996).

4. M.I. Skolnik, *Radar Handbook* (McGraw Hill, New York, NY, 1990) (Chapter 16: Airborne MTI).

5. D. Wehner, *High Resolution Radar* (Artech House, Norwood, MA, 1995).

6. J. Scheer and J. Kurtz, *Coherent Radar Performance Estimation* (Artech House, Norwood, MA, 1993).

7. J. Genova, "Coherent Radar Guided Anti-Ship Missile Hardware Simulator Development Planning Report," NRL Code 5760, February 4, 2003.

8. K. Gerlach and M. Picciolo, "Robust STAP Using Reiterative Censoring," 2003 IEEE Radar Conference, Huntsville, AL.

9. Y. Zhang and H. Wang, "Further Results of ΣΔ-STAP Approach to Airborne Surveillance Radars," 1997 IEEE National Radar Conference, Syracuse, NY.

10. A. Paine, "Application of the Minimum Variance Monopulse Technique to Space-Time Adaptive Processing," IEEE International Radar Conference, 2000, Alexandria, VA.

Appendix A
GENERAL COHERENT SIGNAL PROCESSING FORMALISM

A derivation of the general coherent processed signals is presented. Figure A1 defines the geometry for radar returns consisting of a target at R and ϕ_T and clutter at the same range, spread throughout the beam at angles ϕ_k. Figure A2 illustrates the receiver geometry and defines ΔR. From the figures, the range to each receiver element and its radial speed are

$$R' = R \pm \Delta R \tag{A1}$$

$$R = R_0 + v_R t \tag{A2}$$

$$v_R = -v \cos(\phi_k) \qquad clutter \tag{A3}$$

$$v_R = -v \cos(\phi_T) - v_T \cos(\theta) \qquad target. \tag{A4}$$

Assume the transmitted signal as in Eq. (A5), then the receive signal is as in Eq. (A6):

$$s(t) = \cos[2\pi(f_c + df)t] \tag{A5}$$

$$r(t) = \cos[2\pi(f_c + df)(t - 2R'/c)]. \tag{A6}$$

From the definition of ΔR and the following definitions, the sum and delta signals are formed in the antenna:

$$\lambda = c/(f_c + df) \tag{A7}$$

$$\Phi = (f_c + df)(2\Delta R/c) = (d/\lambda)\sin(\gamma - \phi) \tag{A8}$$

$$\Sigma(t) = \cos[2\pi(f_c + df)(t - 2R/c)] \cdot \cos(2\pi\Phi) \tag{A9}$$

$$\Delta(t) = \sin[2\pi(f_c + df)(t - 2R/c)] \cdot \sin(2\pi\Phi). \tag{A10}$$

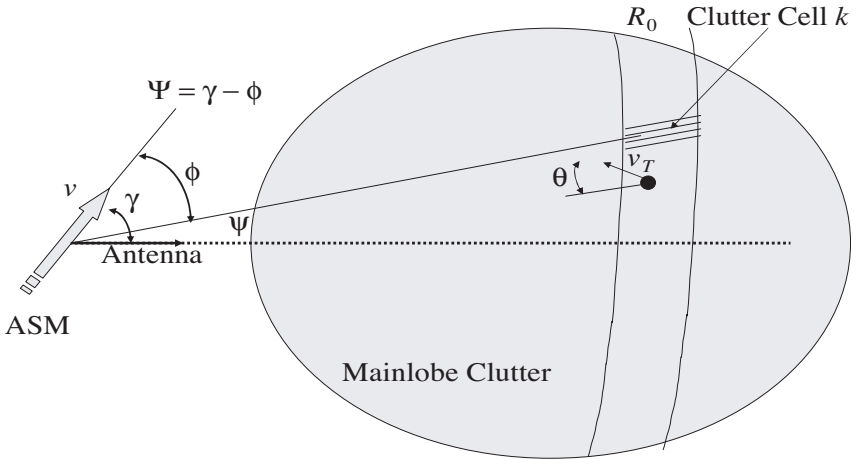

Fig. A1 — Geometry

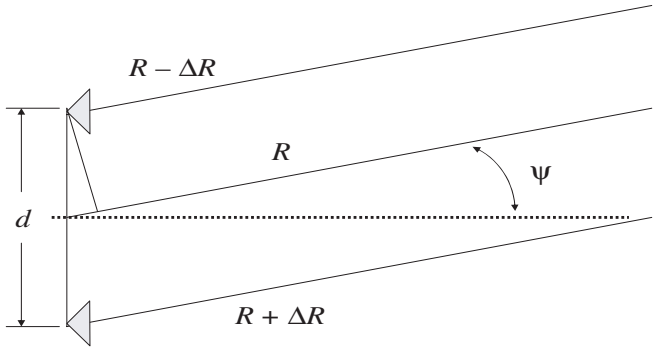

$$\Delta R = (d/2) \cdot \sin(\psi) = (d/2) \cdot \sin(\gamma - \phi)$$

Fig. A2 — Phase monopulse antenna

The signals are next processed to lower the signal to IF (see the mixer of Fig. A3):

$$\Sigma(t) = \cos\left[2\pi(f_0 \cdot t + df \cdot t - 2R_0/\lambda - 2v_R t/\lambda)\right] \cdot \cos(2\pi\Phi) \tag{A11}$$

$$\Delta(t) = -\sin\left[2\pi(f_0 \cdot t + df \cdot t - 2R_0/\lambda - 2v_R t/\lambda)\right] \cdot \sin(2\pi\Phi). \tag{A12}$$

The standard procedure is to use INS and/or signal processing to choose *df* such that the mainlobe clutter (MLC) spectral peak Doppler energy is moved to 0 Hz or

$$df = -(2v/\lambda)\cos(\gamma). \tag{A13}$$

Assuming small angles,

$$\cos(\phi) - \cos(\gamma) = \sin(\gamma - \phi) \cdot \sin(\gamma) \tag{A14}$$

$$\Sigma(t) = \cos\{2\pi[(f_0 \cdot t - 2R_0/\lambda) + (2v \cdot t/\lambda)\sin(\gamma - \phi)\sin(\gamma)]\} \cdot \cos(2\pi\Phi) \tag{A15}$$

$$\Delta(t) = -\sin\{2\pi[(f_0 \cdot t - 2R_0/\lambda) + (2v \cdot t/\lambda)\sin(\gamma - \phi)\sin(\gamma)]\} \cdot \sin(2\pi\Phi). \tag{A16}$$

It is noted that the second term in the brackets is slowly varying within a pulse. Thus, letting the time variable in the second term be $t = p \cdot T = p/PRF$ and defining

$$\beta = (2vT/d)\sin(\gamma), \tag{A17}$$

the input to the heterodyne receiver (see Fig. A4) is approximately

$$\Sigma(t) = \cos\{2\pi[(f_0 \cdot t - 2R_0/\lambda) + (\beta\Phi p)]\} \cdot \cos(2\pi\Phi) \tag{A18}$$

$$\Delta(t) = -\sin\{2\pi[(f_0 \cdot t - 2R_0/\lambda) + (\beta\Phi p)]\} \cdot \sin(2\pi\Phi). \tag{A19}$$

Using the relationships in Fig. A4, the signals at baseband for pulse *p* and range cell R_0 are

$$\Sigma = \exp\left[2\pi i(\beta\Phi p)\right] \cdot \cos(2\pi\Phi) \tag{A20}$$

$$\Delta = -i\exp\left[2\pi i(\beta\Phi p)\right] \cdot \sin(2\pi\Phi). \tag{A21}$$

For convenience, the following combinations are formed for each pulse *p* (0 to *P* – 1):

$$\Sigma + \Delta = \exp\left[2\pi i(\beta\Phi p)\right] \cdot \exp(2\pi i\Phi) \tag{A22}$$

$$\Sigma - \Delta = \exp\left[2\pi i(\beta\Phi p)\right] \cdot \exp(-2\pi i\Phi). \tag{A23}$$

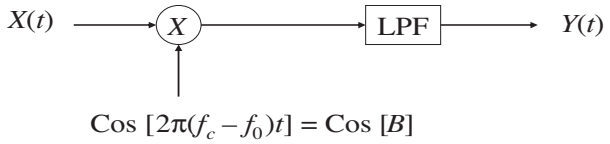

X	$2\pi(f_c - f_0)t = B$	Y
Cos (A)		Cos ($A - B$)
Sin (A)		–Sin ($A - B$)

Fig. A3 — Mixer

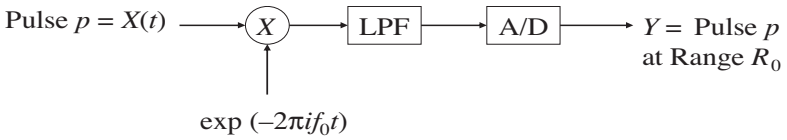

X	Y
$A \cos [2\pi(f_0 t + \Omega)]$	$A \exp (2\pi i \Omega)$
$-A \sin [2\pi(f_0 t + \Omega)]$	$iA \exp (2\pi i \Omega)$

Fig. A4 — Heterodyne receiver

Equations (A22) and (A23) provide the basic information from which the full return can be written for the P pulses at this range cell ($2P$ terms). The full return is a combination of noise (n), clutter, and, possibly, a target. The clutter is a combination of many scatter elements at each angle within the beam, summed over all angles (k). For example, the sum term (Eq. (A22)) (neglecting internal clutter motion) is

$$[\Sigma + \Delta]\ clutter = \Sigma_k \{c_k \exp [2\pi i(\beta \Phi_k p)] \cdot \exp (2\pi i \Phi_k)\}\,. \tag{A24}$$

The target term is of the same form, but it includes the ownship Doppler as well as the ASM-induced Doppler

$$[\Sigma + \Delta]\ target = a \exp [2\pi i(\beta \Phi_T + \alpha_T)p] \cdot \exp (2\pi i \Phi_T)\}\,, \tag{A25}$$

where $\Phi_T = (d/\lambda) \sin (\gamma - \phi_T)$ and

$$\alpha_T = [(2 v_T T) / \lambda] \cdot \cos (\theta)\,. \tag{A26}$$

The difference terms are the same except for the sign of the last exponential (see Eqs. (A22) and (A23)).

Vectors of dimension $2P$ can be formed at each range cell using the P-summed returns and the P-subtracted terms. The general return ($2P$ vector) is

$$X = a \cdot X_T + X_c\,, \tag{A27}$$

where X_T is formed from the target returns and X_c is formed from the clutter plus noise (and, possibly, jamming) terms. The detector output can be defined as the weighted sum of the components or the vector product of X and the weight vector W,

$$z = W^T \cdot X. \tag{A28}$$

Defining the matrix M, the signal power to interference power is

$$SINR = [a^2 \cdot (W^T \cdot X_T) \cdot (W^T \cdot X_T)] \,/\, [(W^T \cdot M \cdot W] \tag{A29}$$

$$M = \langle X_c \cdot X_c^T \rangle. \tag{A30}$$

It is desired to determine the optimal ($2P$) weight vector for the combined (angle and Doppler) processing that maximizes SINR (Eq. (A29)). The standard argument is to insert the identity into the numerator of the expression and use the Cauchy inequality as

$$SINR \;=\; a^2 \cdot [W^T \; M^{1/2} \cdot M^{-1/2} \; X_T \,]^2 \,/\, [(W^T \cdot M \cdot W \,] < a^2 \cdot [\, X_T^T \; M^{-1} \; X_T \,] \,. \tag{A31}$$

The expression for SINR attains the upper limit when the vectors in the numerator are collinear or

$$W = M^{-1} \cdot X_T \,. \tag{A32}$$

Equation (A28) shows that this weight vector effectively cancels the interference (prewhitens the noise) and maximizes the SINR at the target. The various vectors X_T are the steering vectors (steering toward potential targets in both angle and Doppler). Obviously, a set of weights can be formed for all angles and all Doppler values if an estimate of M is available. The estimation of M is the origin of the A in STAP. The various versions of STAP are the proposed methods for estimating M in real time.

Consider a standard processing scheme such that the baseband sum channel signal (P pulses) is Doppler-filtered and the target detected at its peak Doppler (α_T). Next, the ratio is formed (Δ/Σ) at that cell to measure the pointing error (ψ). From Eqs. (A20) and (A21),

$$\Sigma = a \cdot \exp\,[2\pi i(\beta\Phi_T + \alpha_T)p] \cdot \cos\,(2\pi\Phi_T) \tag{A33}$$

$$\Delta(t) = -i\,a \cdot \exp\,[2\pi i(\beta\Phi_T + \alpha_T)p)] \cdot \sin\,(2\pi\Phi_T)\,. \tag{A34}$$

Thus, this approach results in the correct pointing error estimate, but at the wrong Doppler. (This is the same result discussed in Ref. A1.) In this case, the weight vector (of dimension P) is represented by the Fourier transform at $\alpha = p'/P$,

$$W_p = \exp\,(2\pi i\alpha p), \tag{A35}$$

followed by monopulse processing. However, if the target return is near a significant clutter ridge in angle and/or Doppler, it is expected to be difficult to detect and the parameter estimates corrupted.

BIBLIOGRAPHY

A1. J. Genova, “Coherent Radar Guided Anti-Ship Missile Hardware Simulator Development Planning Report,” NRL Code 5760, February 4, 2003.

Appendix B
EXAMINATION OF APPROXIMATIONS

Note 1: The results of Appendix A simplify the expressions. The received signals in Eqs. (A6) include half of the total contribution from the transmitted signals. Equation (A6) should more accurately read

$$ru(t) = \cos\,[2\pi(f_c + df)\,(t - 2R/c)] + \cos\,[2\pi(f_c + df)\,(t - 2R/c + 2\Delta R/c)] \tag{B1a}$$

$$rl(t) = \cos\,[2\pi(f_c + df)\,(t - 2R/c)] + \cos\,[2\pi(f_c + df)\,(t - 2R/c - 2\Delta R/c)]. \tag{B1b}$$

Thus, Eq. (A10) is the same as shown, while Eq. (A9) contains an additive term without the cos (2πΦ). Continuing the derivation, Eqs. (A22) and (A23) should read

$$\Sigma + \Delta = \exp\,[2\pi i(\beta\Phi p)] \cdot \exp\,(\pi i\Phi) \cdot \cos\,(\pi\Phi) \tag{B2}$$

$$\Sigma - \Delta = \exp\,[2\pi i(\beta\Phi p)] \cdot \exp\,(-\pi i\Phi) \cdot \cos\,(\pi\Phi)\,. \tag{B3}$$

In conclusion, the expressions are the same for the Doppler dependence. However, the separate phase factor (fixed over the P pulses) differs by a factor of 2 in the argument, and the terms are amplitude-weighted by a cosine of the angular dependence.

Note 2: At Eqs. (A14)-(A16), the small look angle ($\psi = \gamma - \phi$) approximation was made. This is valid for the larger amplitude portions of the mainlobe clutter (MLC). In general, there will be contributions from the entire antenna beam. This contribution is referred to as sidelobe clutter (SLC) and was used in the body of the report. The Doppler frequency for the general contribution of a target (ship, clutter, decoy, etc.) of speed v_0 at angle θ_0 is

$$f_\alpha = (2v/\lambda) \cdot \{\sin\,(\gamma - \phi) \cdot \sin\,(\gamma) - \cos\,(\gamma) \cdot [1 - \cos\,(\gamma - \phi)]\} + (2v_0/\lambda) \cdot \cos\,(\theta_0)\,. \tag{B4}$$

Since the factor $(2v/\lambda)$ is expected to be large, the SLC smears (via aliasing) over the Doppler region, adding a clutter noise floor contribution. While this clutter is lower than the MLC by the antenna gain squared, it represents a much larger ocean surface area, i.e., clutter scatter cross section. This contribution needs more precise evaluation.

Figure B1 shows the region near the center of the mainlobe. (Doppler is in Hz and angle in degrees for $\gamma = 5$ deg. It is assumed that v_0 is zero.) Figure B2 expands the abscissa to show the entire Doppler pattern. (The amplitude [not shown] is weighted by the individual scatter elements and the antenna pattern.) Figure B3 is the same as Fig. B2, but it is plotted vs the equivalent angle Φ (times 2π and in radians). As seen, the standard STAP analysis deals with sidelooking (or ISAR) processing (γ near 90 deg) while the ASM problem deals with small γ. However, near boresight the equations take a form very similar to the standard STAP expressions.

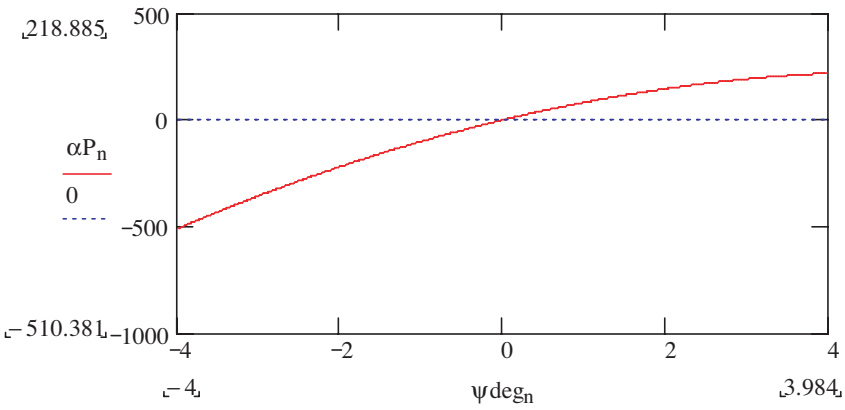

Fig. B1 — Clutter Doppler vs angle off-boresight

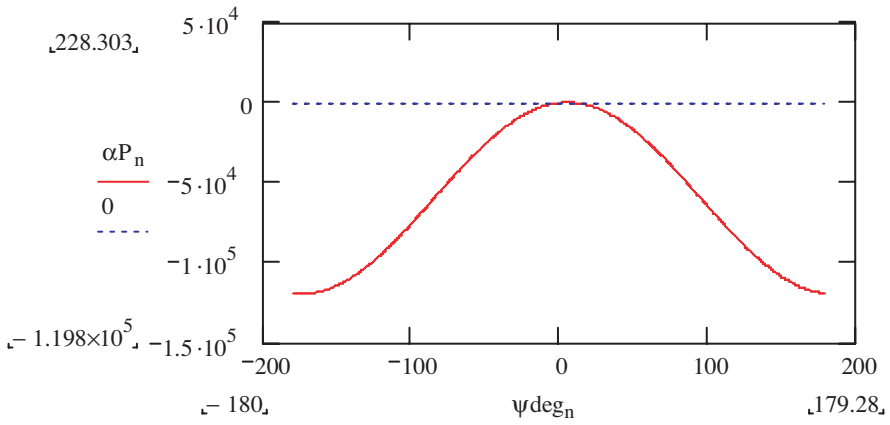

Fig. B2 — Clutter Doppler vs angle

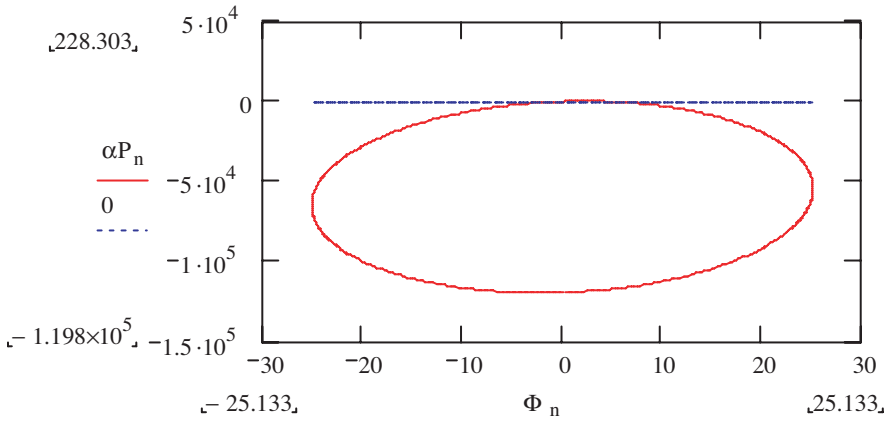

Fig. B3 — Clutter Doppler vs generalized angle